JOURNAL OF MATERIALS SCIENCE 20 (1985) 718–729

Excess nitrogen and discontinuous precipitation in nitrided iron–chromium alloys

P. M. HEKKER, H. C. F. ROZENDAAL, E. J. MITTEMEIJER
Laboratory of Metallurgy, Delft University of Technology, Rotterdamseweg 137, 2628 AL Delft, The Netherlands

FeCr (1.88 and 3.61 wt % Cr) specimens were gas nitrided (10 vol % NH_3/90 vol % H_2 gas mixture at 833 K). The structure after nitriding was studied employing metallographic methods (optical microscopy, hardness measurements), scanning electron microscopy and X-ray diffractometry (residual macrostress determination and phase identification). Further the weight and thickness increases of the specimens during nitriding were determined. Excess nitrogen uptake, discontinuous precipitation and void formation were observed. The amount of excess nitrogen observed in an initial stage of precipitation corresponds well with the predicted amount applying thermodynamics of stressed solids. The occurrence of a discontinuous precipitation reaction at later stages of precipitation was accompanied by the loss of excess nitrogen from the supersaturated ferritic matrix. In this way void formation and changes in the residual macrostress distribution within the specimen during nitriding can be explained. As a result a model is presented for the description of the nitriding behaviour of Fe–Cr alloys.

1. Introduction

Nitriding affords a thermochemical surface treatment for workpieces of steel of great technological importance because of its beneficial effect on the fatigue resistance and/or the tribological and anti-corrosion properties. Chromium is frequently applied as an alloying element because of its affinity for nitrogen. Therefore, as a first step in explaining the response to nitriding of a chromium-alloyed steel matrix, there is an apparent need to understand the nitriding behaviour of iron–chromium alloys. Some peculiar observations have been made in previous work: the occurrence of so-called "excess" nitrogen [1–3] and a discontinuous precipitation reaction [4, 5].

In the present investigation the nitriding behaviour of binary iron–chromium alloys (1.88 and 3.61 wt % Cr) is studied. Metallographic methods (optical microscopy, hardness measurements), scanning electron microscopy and X-ray diffractometry (residual macrostress determination and phase identification) are employed. Further the weight and thickness increases of the specimens on nitriding are determined.

2. Experimental procedures

2.1. Specimen preparation

Rectangular specimens (3 cm × 2 cm; thickness 0.06, 0.25 or 0.5 mm; metallography, thickness and weight measurements) as well as disc-shaped specimens ($\phi = 20$ mm, thickness 2 mm; X-ray diffractometry) of iron (0.0042 at % Ni; 0.0009 at % Cu; 0.0014 at % Mn; <0.01 at % Si; 0.011 at % C; <0.001 at % N, balance Fe) and iron–chromium alloys (1.88 and 3.61 wt % Cr, corresponding to 2.02 and 3.88 at % Cr, respectively) were used. Before nitriding the specimens were mechanically polished (final stage 1 μm diamond), ultrasonically cleaned in alcohol, degreased in trichloroethane and etched in a 2% nital solution.

2.2. Nitriding procedure

Nitriding was performed in a vertical tube furnace (tube and suspension of specimen made of quartz)

0022–2461/85 $03.00 + .12

in a 10 vol% ammonia (Matheson; 99.96 vol%) and 90 vol% hydrogen (Hoek Loos; 99.995 vol%) gas mixture at 833 K (temperature control within 2 K). Both gases were purified by leading them through BTS-catalyst and soda lime subsequently before entering the mixing bottle. The flowrate in the furnace was about 0.8 cm sec^{-1}. Under these conditions no compound (iron nitride) layer formation occurred at the surface.

2.3. Weight measurements

Weight increase as a function of nitriding time was determined by using a Mettler balance type M5SA (accuracy about 5×10^{-6} g).

2.4. Thickness measurements

Thickness increase as a function of nitriding time was determined by using a Millitron 1202 instrument equipped with two ruby feelers (accuracy about 1.5 μm). Each thickness value is the mean of 5 to 10 measurements.

2.5. Metallography

Optical microscopy was performed with a Neophot-2 microscope (Carl Zeiss, Jena). Microhardness profiles were determined applying a Leitz Durimet microVickers hardness tester (applied load 100 g). Each hardness value presented is the mean of 5 to 10 measurements. Scanning electron microscopy was performed with a JEOL JXA 50A instrument.

2.6. X-ray diffractometry

For phase identification, scans over the range 25 to 130° 2θ were made (scan speed about 2° 2θ min^{-1}) employing a Siemens type $F-\omega$ diffractometer equipped with a graphite monochromator in the diffracted beam and using Co$K\alpha$ radiation. The residual macrostress was determined by applying the $\sin^2\psi$ method [6]. To this end the (220) line profile of the iron matrix was recorded according to the preset-time method in steps of 0.025° 2θ employing counting times in the range 20 to 175 sec, depending on the peak intensity. Large portions of the background at both sides of the peak were recorded. The background was interpolated linearly between both extremities. The α_2 component was eliminated by computation [7]. To determine the peak position a parabola was fitted to the corrected intensities by applying a least-squares procedure employing those intensity values larger than 80% of the maximum intensity.

To determine the macrostrain as a function of depth below the surface, layers were removed from the surface by mechanical polishing (final stage 1 μm diamond). Macrostress relaxation effects due to layer removal were corrected for according to [8].

3. Results

3.1. Morphology

Cross-sections of nitrided iron–chromium specimens (1.88 and 3.61 wt% Cr; thickness 0.5 mm) are shown in Figs. 1 and 2. Although the specimens have been fully nitrided, a varying microstructure is observed.

An apparent discontinuous precipitation reaction, starting from grain boundaries, took place in the surface region. This effect is more pronounced for the Fe–3.61 wt% Cr alloy, as compared to the Fe–1.88 wt% Cr alloy. The lamellae-like structure is revealed by scanning electron microscopy (Fig. 3; interlamellar distance about 50 nm). X-ray diffractometry analysis from the surface demonstrated the presence of two phases: chromium nitride (CrN) and α-iron.

Below this surface region a zone is observed where only part (Fe–3.61 wt% Cr) or none (Fe–1.88 wt% Cr) of the crystals is transformed by the discontinuous precipitation reaction. Precipitates in the untransformed crystals (whose presence is also deduced from hardness measurements reported in Section 3.2) are apparently of submicroscopical size. They change the optical constants of the matrix such that this zone containing submicroscopical precipitates can be

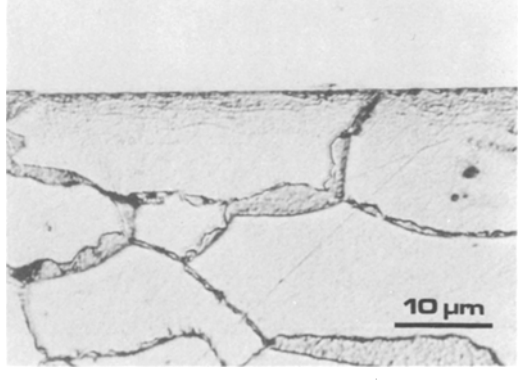

Figure 1 Optical micrograph of a cross-section of a through-nitrided (202 h; 10 vol% NH_3/90 vol% H_2; 833 K) Fe–1.88 wt% Cr specimen (thickness 0.5 mm). Discontinuous precipitation has occurred in regions adjacent to grain boundaries.

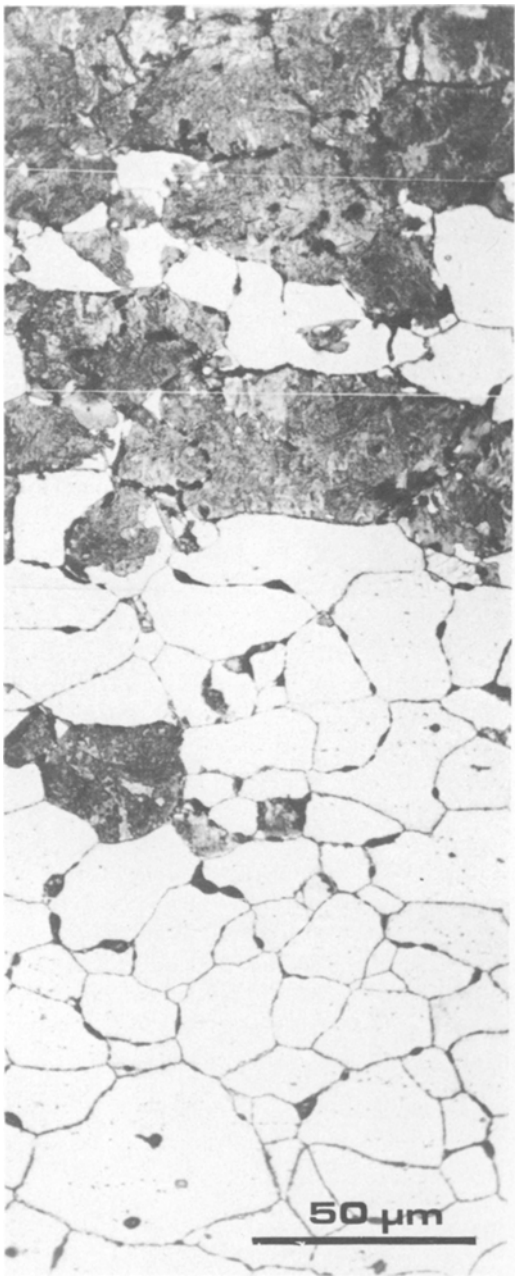

Figure 2 Optical micrograph of a cross-section of a through-nitrided (90 h; 10 vol% NH_3/90 vol% H_2; 833 K) Fe–3.61 wt% Cr specimen (thickness 0.5 mm) showing three zones (i) near the surface all crystals are transformed by discontinuous precipitation; (ii) below the surface layer a zone exists where only part of the crystals are transformed; the remaining crystals contain submicroscopical precipitates (continuous precipitation); (iii) in the centre of the specimen only continuous precipitation has occurred. Voids and grain boundary precipitates can be observed.

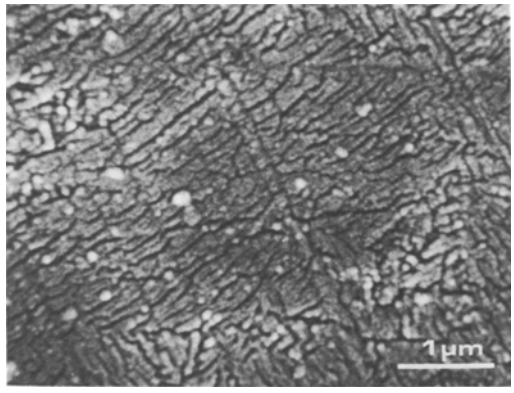

Figure 3 Scanning electron micrograph of a cross-section of a nitrided (2 h; 10 vol% NH_3/90 vol% H_2; 833 K) Fe–3.61 wt% Cr specimen (thickness 0.5 mm) showing the lamellae-like structure of a transformed crystal. The interlamellar distance is of the order 50 nm.

distinguished from un-nitrided material by interference etching applying a vapour-deposited interference filter (Fig. 4, see also Fig. 11 and [9]). The reaction which took place in the untransformed crystals will further be denoted by "continuous precipitation" as compared to the "discontinuous precipitation" reaction indicated above.

Further grain boundary precipitates (Fig. 2; see also Fig. 10a in [10]) and voids at the grain boundaries can be observed (Fig. 5).

3.2. Microhardness profiles

On nitriding the Fe–1.88 wt% Cr alloy the surface hardness increases during the first hours of nitriding (Fig. 6; hardness values determined in grains showing continuous precipitation). After reaching a maximum value the surface hardness decreases on prolonged nitriding. A shallow hardness gradient at the case–core interface is observed.

For the Fe–3.61 wt% Cr alloy distinction was made between the hardness of the zones containing continuous and discontinuous precipitates, respectively. The maximum surface hardness (determined from grains showing continuous precipitation; Fig. 7a) is already reached after the shortest nitriding time; on prolonged nitriding this surface hardness decreases. A very large hardness gradient is observed at the case–core interface. The hardness of the (near-surface) grains showing discontinuous precipitation is significantly lower than that of the grains showing continuous

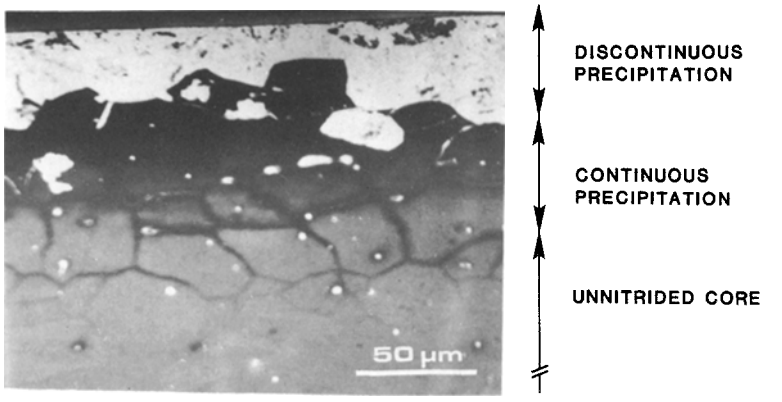

Figure 4 Optical micrograph (monochromatic light (578 nm); vapour-deposited ZnTe interference filter) of a cross-section of a nitrided (2 h; 10 vol% NH_3/90 vol% H_2; 833 K) Fe–3.61 wt % Cr specimen (thickness 0.5 mm). Three regions can be distinguished: (i) a near-surface zone where discontinuous precipitation has occurred; (ii) a zone beneath zone (i), where in the majority of the grains only continuous precipitation has occurred and (iii) the unnitrided core. Regions (ii) and (iii) can be distinguished as a result of interference etching [9].

precipitation (cf. Figs. 7a and b). On prolonged nitriding decrease of this hardness occurs.

3.3. Weight gain

The weight increase (mg N/g Fe) of Fe–3.61 wt % Cr alloys during nitriding is shown in Fig. 8 for three specimens of thickness 0.06, 0.25 and 0.47 mm, respectively. The dashed line, denoted by N_{th}, indicates the expected amount of nitrogen that can be taken up, i.e. the amount of nitrogen that forms stoichiometrical CrN plus the maximum amount of nitrogen that dissolves interstitially in the pure ferrite matrix. The latter value was determined experimentally in a separate experiment, where pure iron was nitrided at 833 K in

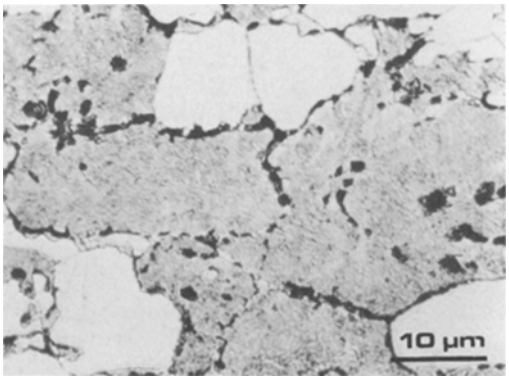

Figure 5 Optical micrograph of a nitrided (200 h; 10 vol % NH_3/90 vol % H_2; 833 K) Fe–3.61 wt % Cr specimen showing voids along grain boundaries in region (ii) (cf. Figs. 2 and 4).

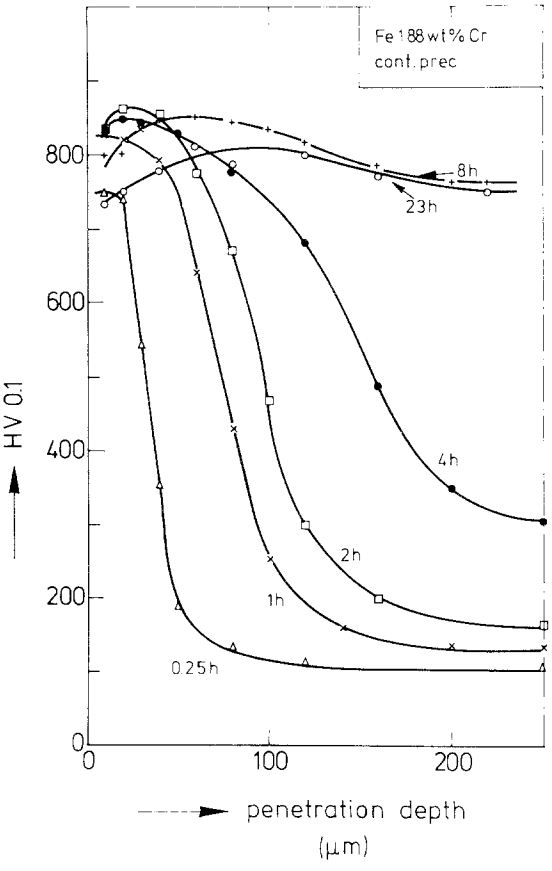

Figure 6 Microhardness profiles (applied load 100 g) for those grains containing continuous precipitates of nitrided (10 vol % NH_3/90 vol % H_2; 833 K) Fe–1.88 wt % Cr specimens (thickness 0.5 mm). The maximum surface hardness is attained after some time of nitriding. Prolonged nitriding thereafter yields a lowering of the surface hardness. No sharp case/core interface develops.

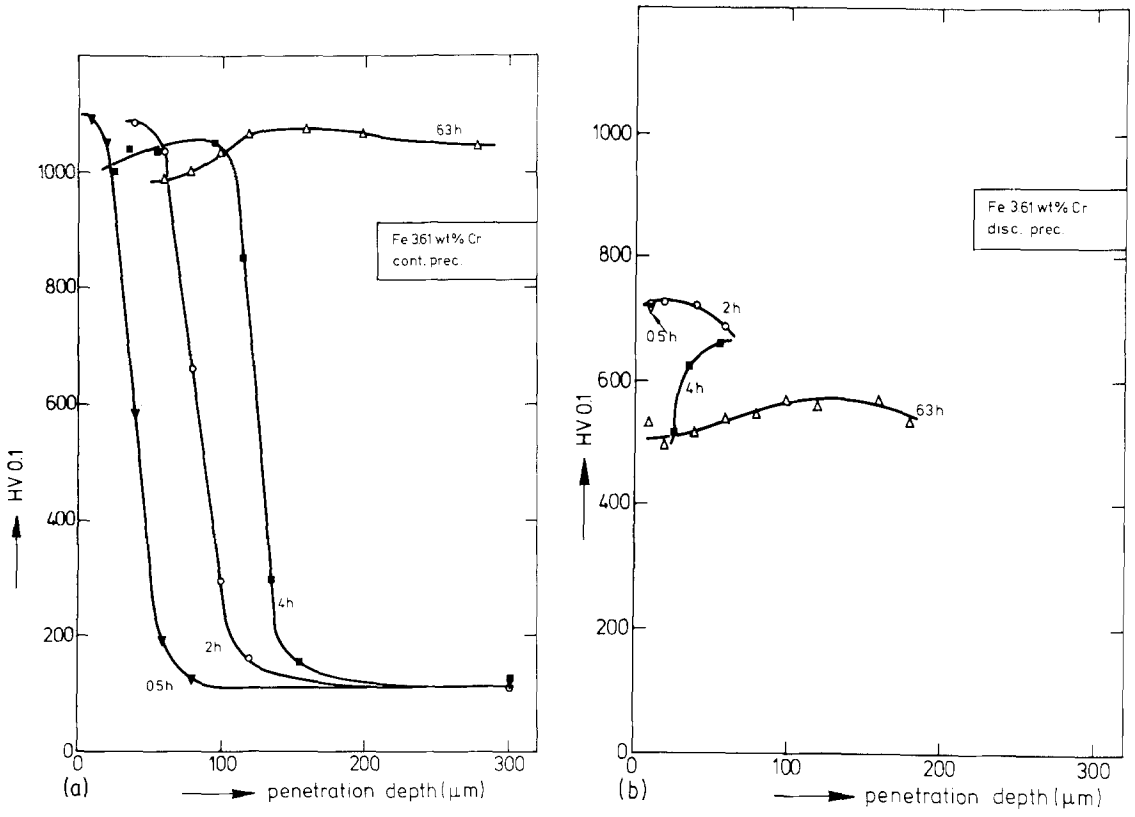

Figure 7 (a) Microhardness profiles (applied load 100 g) for those grains containing continuous precipitates of nitrided (10 vol% NH_3/90 vol% H_2; 833 K) Fe–3.61 wt% Cr specimens (thickness 0.5 mm). The maximum surface hardness is already observed after the shortest nitriding time. Prolonged nitriding yields a lowering of the surface hardness. A sharp case/core interface develops. (b) Microhardness profiles (applied load 100 g) for those grains containing discontinuous precipitates of nitrided (10 vol% NH_3/90 vol% H_2; 833 K) Fe–3.61 wt% Cr specimens (thickness 0.5 mm). Prolonged nitriding yields lower hardness values.

the 10 vol% NH_3/90 vol% H_2 gas mixture, as 0.69 mg N/g Fe.

The total experimentally observed weight increase considerably exceeds the predicted value. "Excess nitrogen" is defined as the total amount of absorbed nitrogen reduced by the "theoretical" (see above) amount of nitrogen. The maximum amount of excess nitrogen depends on specimen thickness (Fig. 9). Further it follows from Fig. 8 that the amount of excess nitrogen decreases on prolonged nitriding.

3.4. Thickness increase

The increase of thickness as a function of nitriding time is shown in Fig. 10 for a Fe–3.61 wt% Cr specimen. It is noted that a significant dilatation starts when the presence of excess nitrogen is certain (after about 10 h of nitriding). On prolonged nitriding dilatation continues although (some) excess nitrogen is lost.

3.5. Residual macrostresses

Macrostress values as a function of depth below the surface are presented in Table I.

In the Fe–1.88 wt% Cr alloy always a "compressive" residual surface stress was found. In

TABLE I Residual macrostresses parallel to the surface of Fe–Cr specimens (thickness 2 mm) after nitriding in a 10 vol% NH_3/90 vol% H_2 gas mixture at 833 K

Chromium content (wt%)	Nitriding time (h)	Depth below the surface (μm)	Residual macrostress (MPa)
		0	126
		35	97
		65	116
		120	371
3.61	63	160	–
		205	–
		245	–
		280	−411
1.88	4	0	−240

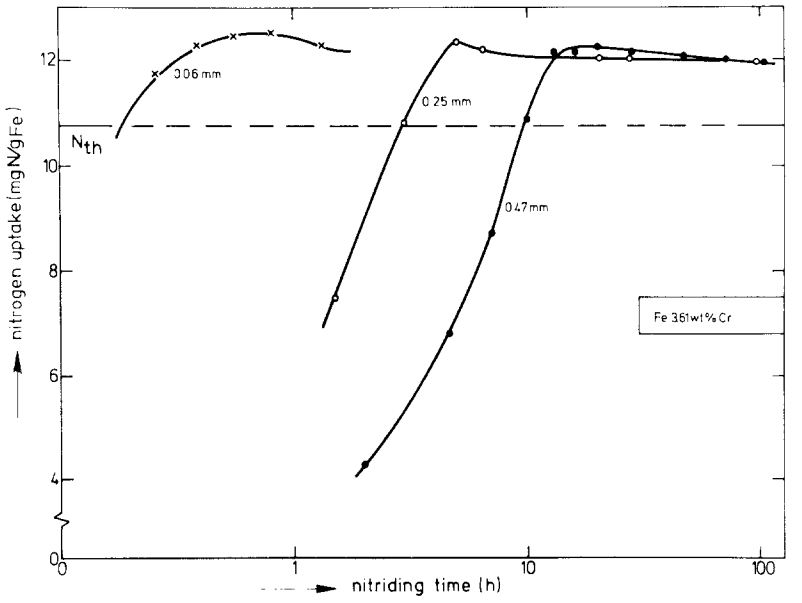

Figure 8 Weight increase during the nitriding (10 vol% NH_3/90 vol% H_2; 833 K) of Fe–3.61 wt% Cr specimens (thickness of 0.06, 0.25 and 0.47 mm, respectively). The dashed line denotes the theoretical amount of nitrogen, N_{th}, to be taken up (cf. Section 3.3). The actual amount of nitrogen absorbed exceeds this value: "excess nitrogen". On prolonged nitriding the amount of excess nitrogen decreases.

the Fe–3.61 wt% Cr specimen, however, a "tensile" residual stress is found down to 120 μm beneath the surface. This region is dominated by discontinuous precipitates (Fig. 11). In the region from 160 to 245 μm no reliable macrostress values could be determined, because the X-ray diffraction line profiles were extremely broadened. In this region a heterogeneous morphology is observed: both grains containing continuous precipitates and grains containing discontinuous precipitates are present (Fig. 11; see also Fig. 2). At still larger depths below the surface a compressive stress was found (Table I).

4. Discussion

4.1. Nitrogen–chromium interaction

Assuming strong nitrogen–chromium interaction (on nitriding all chromium present in the matrix

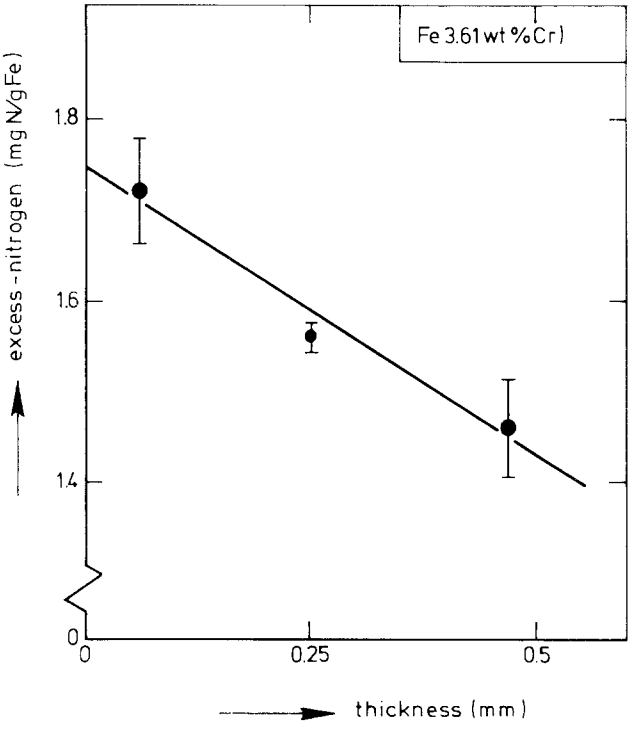

Figure 9 Maximum amount of excess nitrogen (for definition see Section 3.3) in nitrided (10 vol% NH_3/90 vol% H_2; 833 K) Fe–3.61 wt% Cr specimens as a function of specimen thickness. Extrapolation to zero specimen thickness yields the maximum local amount of excess nitrogen (cf. discussion in Section 4.3).

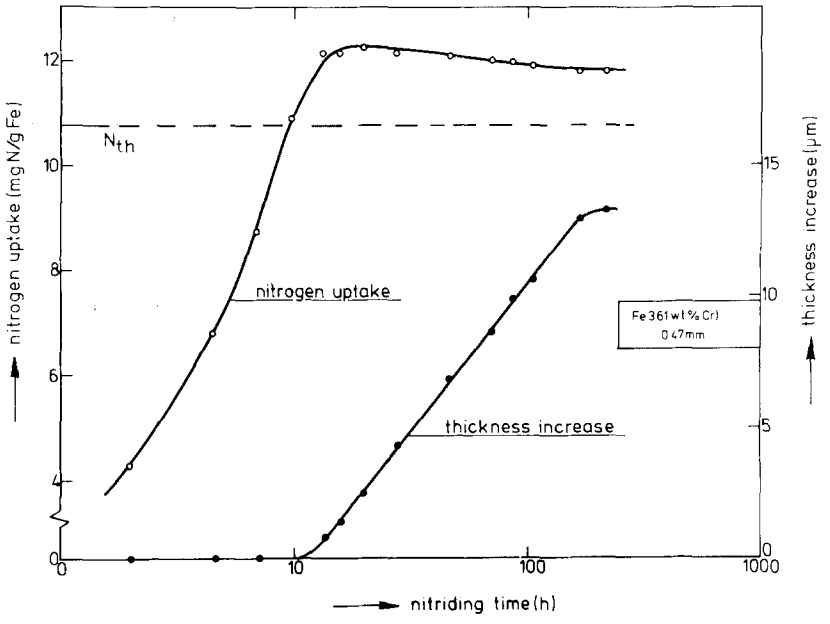

Figure 10 Weight increase and thickness increase during nitriding (10 vol% NH_3/90 vol% H_2; 833 K) a Fe–3.61 wt% Cr specimen (thickness 0.47 mm). An appreciable thickness increase occurs when the maximum weight increase is passed.

is immediately bound to nitrogen; inward diffusion of nitrogen is rate determining) a model originally applied to internal oxidation [11] can be adopted. Characteristics of this model are:

(i) The maximal surface hardness is attained at the start of the nitriding.

(ii) A sharp case–core interface occurs and the nitriding (case) depth, Δz_{case}, can be calculated from:

$$(\Delta z_{case})^2 = 2\left\{\frac{[N]^s_\alpha D^N_\alpha t}{[Cr]}\right\} \qquad (1)$$

where $[N]^s_\alpha$ = nitrogen concentration at the surface in the iron matrix (0.69 mg N/g Fe (see Section 3.3.) $\hat{=}$ 0.274 at%); [Cr] = chromium concentration in the specimen; D^N_α = diffusion coefficient of nitrogen in pure ferrite (8.69×10^{-12} m^2 sec^{-1} [12]) and t = nitriding time, all at 833 K.

The experimental nitriding depth is determined as the distance from the surface, where the microhardness equals half that of the surface (continuous precipitation; cf. Figs. 6 and 7a). The bold and dashed lines in Fig. 12 correspond to the experimental and theoretical (according to Equation 1) nitriding depths. The considerable difference between the theoretical prediction and the experiment for the Fe–1.88 wt% Cr alloy reflects that chromium is an element of intermediate strength

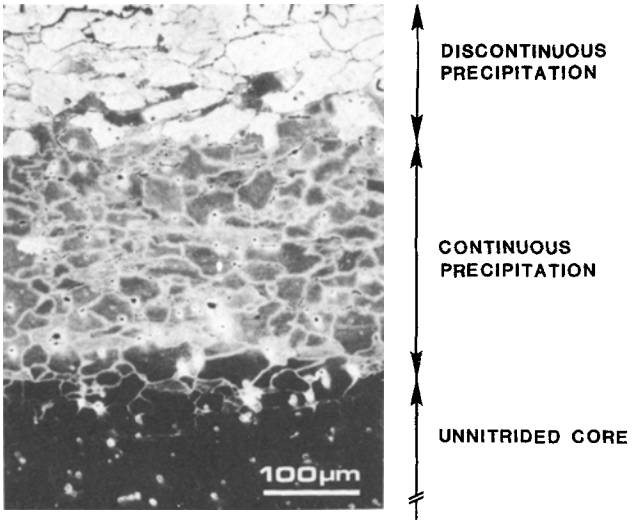

Figure 11 Optical micrograph (monochromatic light (546 nm); vapour-deposited ZnTe interference filter [9]) of a nitrided (63 h; 10 vol% NH_3/90 vol% H_2; 833 K) Fe–3.61 wt% Cr specimen (thickness 2 mm). From this specimen residual-stress data gathered in Table I were obtained.

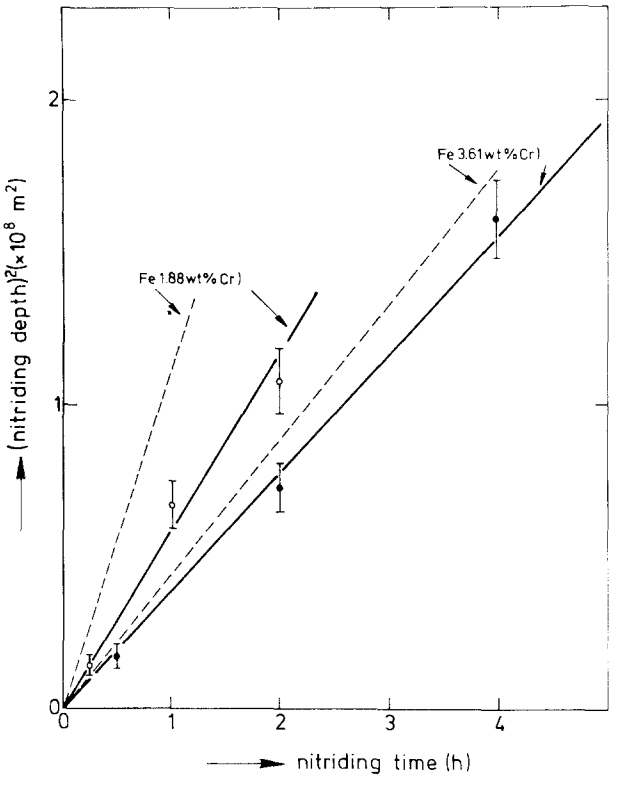

Figure 12 Nitriding depth as a function of nitriding time. The dashed lines denote the theoretical result assuming strong nitrogen–chromium interaction. The bold lines represent the experimental results (see discussion in Section 4.1).

for nitriding: the nitrogen–chromium interaction can change from strong to weak by lowering the chromium content of the alloy [13]. In this sense it can be remarked that the microhardness in the core of the specimen is equal to the initial value for the Fe–3.61 wt % Cr alloy at nitriding times where already an increasing core hardness is observed for the Fe–1.88 wt % Cr alloy (cf. Figs. 6 and 7a).

4.2. Discontinuous precipitation

The following type of discontinuous precipitation reaction appears appropriate for the present system (see review on discontinuous precipitation reactions in [14]):

$$\alpha' + \beta' \rightarrow \alpha + \beta \qquad (2)$$

where β' denotes coherent CrN precipitates in a supersaturated matrix (α'). The reaction consists of the replacement of coherent CrN precipitates by CrN lamellae ($\beta' \rightarrow \beta$) under simultaneous elimination of the supersaturation of the matrix ($\alpha' \rightarrow \alpha$). The following changes in free energy of the specimen contribute to the driving force for this process:

(i) reduction of the interfacial free energy;

(ii) reduction of the chemical free energy (elimination of the supersaturation) and

(iii) reduction of free energy as a result of stress relaxation. (In the α' matrix large stress fields corresponding to the coherent precipitates are present).

General characteristics of this type of discontinuous precipitation are [14]

(a) The morphology of the discontinuous precipitation is lamellae-like.

(b) The reaction takes place in supersaturated grains containing continuous precipitates.

(c) The initiation of the reaction requires mobile grain boundaries.

With regard to the above characteristics the present experiments provide the following results:

(a) The lamellae-like structure was revealed by optical and scanning electron microscopy (Fig. 3).

(b) The presence of continuous precipitates was indicated by the very high microhardness values (Figs. 6 and 7a) and by reflectivity measurements (Fig. 4). The presence of excess nitrogen was revealed by weighing of the specimens (Fig. 8). Indeed on prolonged nitriding the amount of excess nitrogen decreased indicating the progress of discontinuous precipitation. The excess nitrogen could diffuse outward as well as precipitate at

grain boundaries thereby causing the occurrence of voids ($2\ [N]_\alpha \rightarrow N_2$; cf. Fig. 5; for further discussion see Section 4.3.).

(c) Figs. 1 and 2 show that the discontinuous precipitation reaction was initiated at grain boundaries. The discontinuous precipitation reaction did not take place in the whole specimen even after through-nitriding: Fig. 2 shows a fully nitrided specimen (3.61 wt% Cr; nitriding time = 90 h). Only in the surface regions complete discontinuous precipitation occurred. According to our opinion this is caused by the immobilization (pinning) of grain boundaries by precipitates at the grain boundaries at larger depths (cf. Fig. 2). Nitriding proceeds faster along grain boundaries than through the bulk (cf. Fig. 4). Therefore at larger penetration depths grain-boundary precipitates have time to develop before the bulk diffusion front arrives, thus preventing the initiation of the discontinuous precipitation reaction there.

Fig. 2 (fully nitrided Fe–3.61 wt% Cr) and Fig. 1 (fully nitrided Fe–1.88 wt% Cr) demonstrate that the extent of the discontinuous precipitation depends on the chromium content. This result is consistent with our previously reported data that with low chromium concentrations no discontinuous precipitation occurred [4].

4.3. Excess nitrogen

The occurrence of excess nitrogen was reported previously for Fe–Ti alloys [15–17]. The nitrided microstructure described consisted of a ferrite matrix with coherent TiN platelets along (100) planes of the matrix. The occurrence of excess nitrogen in Fe–Cr alloys was suggested previously from experiments with chromium-alloyed steel [3]. It also follows from previous transmission-electron microscopical work [5, 18] that the microstructure of nitrided FeCr alloys (for the crystals showing continuous precipitation) consists of a ferrite matrix with coherent CrN platelets. It is remarked that these data and interpretations, as reported elsewhere, do not exclude that the very initial stage of precipitation comprises a substitutional–interstitial solute–atom clustering (corresponding to Guinier–Preston zone formation) [19] but a conclusive proof for such a phenomenon has not been obtained until now*. It should however be recognized that whatever terminology is preferred, this does not affect in principle the interpretation given in this paper; here the name "continuous precipitation" is assigned to the initial stage of precipitation.

There is disagreement with respect to the location of the excess nitrogen (in Fe–Ti alloys). Excess nitrogen has been claimed to be adsorbed at the edges or surfaces of the platelets [15, 17] or has been ascribed to a dilatation of the matrix, thus enhancing the nitrogen solubility of the ferrite [16]. It has been experimentally confirmed indeed that an average lattice dilatation of a matrix containing misfitting second-phase particles can occur [20]. At present it is impossible to reject either of the above possibilities. In any case both theories ascribe the occurrence of excess nitrogen to the presence of long-range strain fields around coherent precipitates† and in fact may supplement each other (see discussion in [21]).

As the discontinuous precipitation reaction proceeds excess nitrogen has to be removed from the microstructure. Further, coarsening of the continuous precipitates‡ in the core of the specimen (where no appreciable discontinuous precipitates occur; see Section 4.2) leads to a restriction of the strain fields around the precipitates and this contributes also to the loss of excess nitrogen atoms. These nitrogen atoms can diffuse outward (in the near-surface region) or segregate at (sub)grain boundaries and coagulate to molecular nitrogen gas, $2\ [N]_\alpha \rightarrow N_2$§, thereby causing voids.

*The presence of streaks through electron diffraction spots from the matrix is not sufficient to prove the occurrence of clustering since matrix and precipitate spots can coincide in an early stage of precipitation (the streaks may then be associated with size/strain effects). For example, for a thin foil of a nitrided specimen of an Fe–Cr alloy transmission electron microscopy did not reveal separate precipitate diffraction spots (but streaks were present), whereas an extraction replica of the same specimen allowed a positive identification of CrN precipitates [18].

†Hence it is unlikely that the excess nitrogen is associated with the discontinuous precipitates, because (i) the discontinuous precipitation reaction is accompanied with a large decrease of the nitride/ferrite interfacial area and (ii) the misfit between "discontinuous" nitride and ferrite is compensated dominantly by dislocations (incoherent precipitate) which corresponds to the presence of short-range strain fields.

‡The general occurrence of coarsening of continuous precipitates is indicated by the decrease of hardness on prolonged nitriding as observed in Figs. 6 and 7a for the surface region.

§It should be noted here that there always exists a tendency for this reaction because the equilibrium pressure of nitrogen gas corresponding to the nitriding gas mixture employed is very high. Void formation was observed and explained in this way on producing nitrogen austenite [22] and iron nitrides [9].

Eventually, after coalescence of the voids, channel formation at the grain boundaries occurs (Fig. 5). Near the surface nitrogen gas may then leave the specimen through boundaries in open contact with the surface. The remaining nitrogen gas within the specimen causes the appreciable dilatation of the specimen observed (Fig. 10)[¶]. In this connection it is interesting to note that a significant thickness increase was only observed after an appreciable time of nitriding had elapsed and that the thickness increase continued even after the specimen was fully nitrided (Fig. 10).

The amount of excess nitrogen as determined by weighing (cf. Section 3.3) is an average over the thickness of the specimen. While the core of the specimen is not yet fully nitrided, the progress of discontinuous precipitation near the surface can already lead to loss of excess nitrogen atoms (see above). This explains the observation of a maximum in the curve of weight gain against nitriding time (Fig. 8). Note however that after very long nitriding times, excess nitrogen is still observed since (i) discontinuous precipitation only occurs completely near the surface (see Section 4.2) and (ii) nitrogen gas can not escape from larger penetration depths (see above).

The maximum local amount of excess nitrogen to be absorbed may be obtained by the determination of the maximum average amount of excess nitrogen, as determined by weighing, as a function of specimen thickness and extrapolation to zero specimen thickness. Thus it is obtained (Fig. 9) to be 1.75 mg N/g Fe.

Ascribing the presence of excess nitrogen to the presence of long-range strain fields within the α-iron matrix, induced by the misfit between the coherent precipitates and the matrix (see the above discussion), a theoretical estimate of the amount of excess nitrogen may be obtained from the thermodynamics of stressed solids [16, 3]. In the presence of a hydrostatic stress component σ the enhanced nitrogen content C_N^α of the α-iron matrix, as compared to the equilibrium content $C_{0,N}^\alpha$, follows from [23]

$$C_N^\alpha = C_{0,N}^\alpha + C_{\text{excess N}}^\alpha = C_{0,N}^\alpha \exp\{\sigma \bar{V}_N / RT\} \quad (3)$$

where $C_{\text{excess N}}^\alpha$ denotes the amount of excess nitrogen as defined in Section 3.3, R = gas constant, T = absolute temperature, $\bar{V}_N$ = molal volume of nitrogen in α-iron and σ is given by [24]

$$\sigma = \frac{4G_\alpha}{1 + \frac{4}{3}G_\alpha K_{CrN}} \epsilon_m Z_{CrN} \quad (4)$$

where G_α = shear modulus of α-iron, K_{CrN} = compressibility of CrN, Z_{CrN} = mole fraction CrN and the linear misfit parameter ϵ_m is calculated from

$$\epsilon_m = \frac{1}{3}\frac{\bar{V}_{CrN} - \bar{V}_\alpha}{\bar{V}_\alpha} = \frac{1}{3}\frac{\frac{1}{4}a_{CrN}^3 - \frac{1}{2}a_\alpha^3}{\frac{1}{2}a_\alpha^3} \quad (5)$$

where $\bar{V}$ and a denote the volume of 1 mole material and the corresponding unit cell parameter, respectively (in [3] ϵ_m was indicated incorrectly, but the data given were calculated correctly). Data for the constants in Equations 3 to 5 are taken from [16] and [25] (the compressibility of CrN was set equal to that of TiN; the calculated results are not very sensitive to this rough approximation: a change of a factor of 2 in K_{CrN} only causes a change of 20% in $C_N^\alpha / C_{0,N}^\alpha$). Then it is obtained for the theoretical ratio $(C_N^\alpha / C_{0,N}^\alpha)_{th}$

$$(C_N^\alpha / C_{0,N}^\alpha)_{th} = 3.8 \quad (6)$$

which can be compared with the experimental ratio $(C_N^\alpha / C_{0,N}^\alpha)_{exp}$ as obtained from the data presented above ($C_{0,N}^\alpha$ = 0.69 mg N/g Fe (see Section 3.3); $C_{\text{excess N}}^\alpha$ = 1.75 mg N/g Fe (Fig. 9))

$$(C_N^\alpha / C_{0,N}^\alpha)_{exp} = 3.5 \quad (7)$$

In view of the assumptions made, a good correspondence exists between the theoretical and the experimental result.

It should be realized that the experimental ratio, $(C_N^\alpha / C_{0,N}^\alpha)_{exp}$, is based on an extrapolation of the experimental amount of excess nitrogen, $C_{\text{excess N}}^\alpha$, to zero thickness of the specimen (Fig. 9). Thus the complication due to the presence of a residual stress profile within the specimen evoked by a non-nitrided core (see discussion in [3]) is avoided.

4.4. Development of residual macrostresses

On nitriding the nitrided case tends to expand, which process is counteracted by the unnitrided core. As a result normally a compressive residual stress develops near the surface while a tensile

[¶] Only a small part of the thickness increase can be caused by the formation of CrN. The volume expansion caused by CrN formation is 1.7% [4], whereas the observed volume expansion (assuming isotropic expansion) is 8.7% (3 × 2.9%; see Fig. 10).

residual stress evolves in the core [26]*. However for the nitrided Fe–3.61 wt% Cr alloy a tensile residual stress is found in the region adjacent to the surface (Table I). This finding can be explained as follows:

The discontinuous precipitation process, which takes place predominantly in the near-surface region, causes relaxation of the residual stresses present there at the moment of transformation (Equation 2) (cf. recrystallization processes). On prolonged nitriding the zone showing predominantly continuous precipitation continues to develop below the transformed one and consequently will tend to expand analogously as discussed above, which process is counteracted by the (now) transformed (relaxed) surface layer and the unnitrided core. As a result tensile stresses can be expected to develop in the near-surface layer and the core whereas a compressive stress can be expected to occur in the zone of continuous precipitation. Further the tensile nature of the residual surface stress can be enhanced by the occurrence of nitrogen gas precipitation along grain boundaries in the core of the specimen at later stages of nitriding (see discussion in Section 4.3) which process tends to expand the core relatively.

The above picture corresponds with the experimental finding for the Fe–3.61 wt% Cr alloy (Table 1). In the Fe–1.88 wt% Cr alloy discontinuous precipitation occurred only partly in the near-surface region. (The transformation (Equation 2) was observed only near the grain boundaries, Fig. 1). Consequently the original compressive residual surface stress was not relieved sufficiently and a residual surface stress of compressive nature was still observed (Table I).

5. Conclusions: a model for the nitriding behaviour of iron–chromium alloys

1. The nitriding response depends on the chromium content of the alloy. On nitriding at 833 K in a 10 vol% NH_3/90 vol% H_2 gas mixture a strong nitrogen–chromium interaction occurs in the Fe– 3.61 wt% Cr alloy, whereas a nitrogen–chromium interaction of intermediate strength is observed for the Fe–1.88 wt% Cr alloy.

2. On nitriding initially a nitrided scale consisting of a ferritic matrix containing continuous chromium–nitride precipitates of submicroscopical size develops. Due to the long-range strain fields surrounding the coherent precipitates the ferrite matrix is supersaturated with nitrogen: excess nitrogen.

3. In the surface region of the specimen a discontinuous precipitation reaction, resulting in a lamellae-like structure of ferrite and chromium nitride, can occur starting from the grain boundaries. At larger penetration depths the development of grain boundary precipitates prevents initiation of the discontinuous precipitation reaction there.

4. On prolonged nitriding both the progress of discontinuous precipitation (predominantly in the near-surface region) and the coarsening of the continuous precipitates (predominantly present at larger penetration depths) cause the initially dissolved excess nitrogen atoms to diffuse outward or to segregate at grain boundaries, $2\,[N]_\alpha \rightarrow N_2$, thereby producing voids containing nitrogen gas. Coalescence of these voids leads to channel formation at the grain boundaries. Void/channel formation is accompanied with a significant volume increase of the specimen.

5. The discontinuous precipitation reaction in the surface layer is accompanied with relaxation of the compressive residual surface macrostress initially provoked by the interaction between the nitrided case, which tends to expand, and the unnitrided core. Then, on prolonged nitriding further development of the zone predominantly containing continuous precipitates (at larger penetration depths) induces a tensile residual surface macrostress. The tensile nature of the residual surface stress is enhanced by the tendency to volume increase of the core as the result of void/channel formation at later stages of nitriding. These residual macrostress effects are not fully experienced in the Fe–1.88 wt% Cr alloy because the discontinuous precipitation reaction transforms the near-surface region only partly.

Acknowledgements

The authors are indebted to Professor B. M. Korevaar for stimulating discussions and critical reading of the manuscript and to Messrs P. F. Colijn, P. J. van der Schaaf and D. P. Nelemans for skilful experimental assistance. Dr Ir. Th. H. de Keijser and Ing. N. M. van der Pers provided X-ray diffraction facilities. Financial support of the

*A compressive residual surface stress is considered to be of beneficial influence on the fatigue resistance of nitrided workpieces whereas a tensile residual surface stress is thought to have a detrimental effect [27].

Foundation for Fundamental Research of Matter (FOM) is gratefully acknowledged.

References

1. E. T. TURKDOGAN and S. IGNATOWICZ, *J. Iron Steel Inst.* **188** (1958) 242.
2. J. R. ATANASSOVA, *Härterei-Tech. Mitt.* **31** (1976) 325.
3. E. J. MITTEMEIJER, H. C. F. ROZENDAAL, P. F. COLIJN, P. J. VAN DER SCHAAF and R. Th. FURNÉE, Proceedings of the Conference on Heat Treatment 1981, Birmingham, UK, 1981 (The Metals Society London, 1983) p. 107.
4. E. J. MITTEMEIJER, A. B. P. VOGELS and P. J. VAN DER SCHAAF, *J. Mater. Sci.* **15** (1980) 3129.
5. B. MORTIMER, P. GRIEVESON and K. H. JACK, *Scand. J. Met.* **1** (1972) 203.
6. H. P. KLUG and L. E. ALEXANDER, "X-Ray Diffraction Procedures", 2nd edn (John Wiley and Sons, New York, 1974) p. 755.
7. R. DELHEZ and E. J. MITTEMEIJER, *J. Appl. Crystallogr.* **8** (1975) 609.
8. M. G. MOORE and W. P. EVANS, *SAE Trans.* **66** (1958) 340.
9. P. F. COLIJN, E. J. MITTEMEIJER and H. C. F. ROZENDAAL, *Z. Metallkd.* **74** (1983) 620.
10. E. J. MITTEMEIJER, *Härterei-Tech. Mitt.* **36** (1981) 57.
11. J. L. MEIJERING, "Advances in Material Research", Vol. 5 (Wiley Interscience, New York, 1971) p. 1.
12. J. D. FAST and M. B. VERRIJP, *J. Iron Steel Inst.* **176** (1954) 24.
13. B. J. LIGHTFOOT and D. H. JACK, Proceedings of the Conference on Heat Treatment, 1973 (The Metals Society, London, 1975) p. 59.
14. D. B. WILLIAMS and E. P. BUTLER, *Int. Met. Rev.* **26** (1981) 153.
15. D. H. JACK, *Acta Metall.* **24** (1976) 137.
16. H. H. PODGURSKI and F. N. DAVIS, *ibid.* **29** (1981) 1.
17. D. S. RICKERBY, A. HENDRY and K. H. JACK, Proceedings of the Conference on Heat Treatment 1981 Birmingham, UK, 1981 (The Metals Society, London 1983) p. 130.
18. V. A. PHILLIPS and A. U. SEYBOLT, *Trans. AIME* **242** (1968) 2415.
19. K. H. JACK, Proceedings of the Conference on Heat Treatment, 1973 (The Metals Society, London, 1975) p. 39.
20. E. J. MITTEMEIJER, P. VAN MOURIK and Th. H. DE KEIJSER, *Phil. Mag. A* **43** (1981) 1157.
21. E. J. MITTEMEIJER, Proceedings of the Conference on Heat Treatment 1981 Birmingham, UK, 1981 (The Metals Society, London, 1983). p. 164.
22. E. J. MITTEMEIJER, M. VAN ROOYEN, I. WIERSZYLLOWSKI, H. C. F. ROZENDAAL and P. F. COLIJN, *Z. Metallkd.* **74** (1983) 473.
23. J. C. M. LI, R. A. ORIANI and L. S. DARKEN, *Z. Phys. Chem.* **49** (1966) 271.
24. O. RICHMOND, as cited in [16].
25. W. B. PEARSON, "A Handbook of Lattice Spacings and Structures of Metals and Alloys", Vol. 1 (Pergamon Press, London, 1958) p. 625.
26. E. J. MITTEMEIJER, Proceedings of the TMS/AIME Symposium on Case-Hardened Steels: Microstructural and Residual Stress Effects, Atlanta, Georgia, USA, March 1983 (TMS/AIME, 1984).
27. E. J. MITTEMEIJER, *J. Heat Treating* **3** (1983) 114.

Received 29 December 1983
and accepted 30 April 1984